Formation of laser-induced periodic surface structures on niobium by femtosecond laser irradiation

Pan Cabo, Aldara; Dias, A.; Gomez-aranzadi, M.; Olaizola, S. M.; Rodriguez, A.

Published in:
Journal of Applied Physics

DOI:
10.1063/1.4873459

Publication date:
2014

Formation of laser-induced periodic surface structures on niobium by femtosecond laser irradiation

A. Pan, A. Dias, M. Gomez-Aranzadi, S. M. Olaizola, and A. Rodriguez

Citation: Journal of Applied Physics **115**, 173101 (2014); doi: 10.1063/1.4873459
View online: http://dx.doi.org/10.1063/1.4873459
View Table of Contents: http://scitation.aip.org/content/aip/journal/jap/115/17?ver=pdfcov
Published by the AIP Publishing

Formation of laser-induced periodic surface structures on niobium by femtosecond laser irradiation

A. Pan,[1,2] A. Dias,[1,2] M. Gomez-Aranzadi,[1,2] S. M. Olaizola,[1,2] and A. Rodriguez[1]
[1]*CIC microGUNE, Goiru Kalea 9 Polo Innovación Garaia, 20500 Arrasate-Mondragón, Spain*
[2]*CEIT-IK4 and Tecnun, University of Navarra, Manuel Lardizábal 15, 20018 San Sebastián, Spain*

(Received 19 December 2013; accepted 15 April 2014; published online 1 May 2014)

The surface morphology of a Niobium sample, irradiated in air by a femtosecond laser with a wavelength of 800 nm and pulse duration of 100 fs, was examined. The period of the micro/nanostructures, parallel and perpendicularly oriented to the linearly polarized fs-laser beam, was studied by means of 2D Fast Fourier Transform analysis. The observed Laser-Induced Periodic Surface Structures (LIPSS) were classified as Low Spatial Frequency LIPSS (periods about 600 nm) and High Spatial Frequency LIPSS, showing a periodicity around 300 nm, both of them perpendicularly oriented to the polarization of the incident laser wave. Moreover, parallel high spatial frequency LIPSS were observed with periods around 100 nm located at the peripheral areas of the laser fingerprint and overwritten on the perpendicular periodic gratings. The results indicate that this method of micro/nanostructuring allows controlling the Niobium grating period by the number of pulses applied, so the scan speed and not the fluence is the key parameter of control. A discussion on the mechanism of the surface topology evolution was also introduced. © *2014 AIP Publishing LLC*.
[http://dx.doi.org/10.1063/1.4873459]

I. INTRODUCTION

The generation of periodic subwavelength structures provides a simple way to control the aesthetic, functional, and protective surface properties of materials. In this context, laser micro- and nano-structuring techniques are getting increased interest for this purpose. Among the entire laser surface structuring techniques, direct femtosecond laser irradiation allows overcoming the limitations imposed by the diffraction limit[1] in the definition of structures with periods below the incident laser wavelength. Consequently, Femtosecond Laser Induced Periodic Surface Structures (fs-LIPSS) stand out as one of the most actively studied approaches. Fs-LIPSS can be categorized[2] into Low Spatial Frequency LIPSS (LSFL), with orientation perpendicular to the laser beam polarization and periods close to the incident wavelength, and High Spatial Frequency LIPSS (HSFL), that appear with orientations both parallel and perpendicular to beam polarization, and periods that show values much smaller than those of LSFL, even reaching tens of nanometers.

In spite of the numerous literature aimed at discerning the HSFL generation mechanism and the reduction of the LSFL period compared to the incident laser wavelength,[3–13] many uncertainties still arise, which means that further experimental and theoretical research is needed to establish an accurate model.

Since a decade ago, fs-LIPSS have been explored in metals.[3–5,8–12,14] However, the formation of fs-LIPSS in Niobium (Nb) has not yet been reported to the best of our knowledge. The generation of micro/nanopatterned Nb surfaces can provide multiple advantages specially regarding the Nb uses in applications such as electrodes for sensors[15,16] and load-bearing bone implants.[17,18] In the case of medical implants, an appropriate corrugation is essential to yield mechanical interlocking of bone for improved clinical performance of endosseous implants, to mimicry of local cellular environments and favor the process of rapid bone formation for osseointegration. On the other hand, the patterning of Nb used as electrode material enhances the electrical properties.

In the present paper, we address the generation of LIPSS by linearly polarized fs-laser irradiation of Niobium in air.

II. EXPERIMENTAL

A femtosecond laser micro/nanomachining tool was employed for the LIPSS experiments. A Ti:Sapphire laser system consisting of a mode-locked oscillator and a regenerative amplifier was used to generate 100 fs pulses with a central wavelength of 800 nm and a repetition rate of 1 kHz. The pulse energy was adjusted with a two-step setup: A constant attenuator consisting of several neutral density filters and a variable attenuator formed by a half-wave plate and a low dispersion polarizer. The 12 mm diameter laser beam was focused on the sample using a 10× microscope objective with a NA of 0.3. This objective, together with a CCD camera, was used for online monitoring of the laser writing process. The layout of the experimental setup is shown in Figure 1.

The irradiated material was a polished bulk Niobium disc with a RMS surface roughness of 2.08 nm. Microstripes of 15 mm long were written on the surface of the Nb probe with a fixed pulse energy of 3 μJ in order to generate the LIPSS. The sample was placed in a motorized XYZ stage, which allows controlling the number of laser shots applied by varying the XY scan speed, and the laser fluence by changing the distance between the objective and the sample (defocusing distance). The range of scanning speeds tested is between 0.01 and 1.00 mm·s^{-1}. The values of the laser fluence are between 29 and 53 mJ·cm^{-2}.

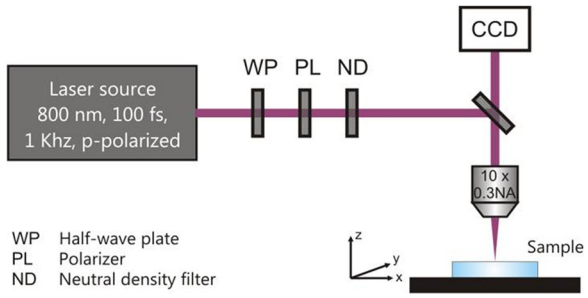

FIG. 1. Schematic layout of the femtosecond laser micro/nanomachining setup.

The Nb topography was inspected by Field Emission Scanning Electron Microscopy (FESEM), Atomic Force Microscopy (AFM) in tapping mode and contact surface profilometry. A free and open source software (Gwyddion) was used to perform the two dimensional Fast Fourier Transform of the micrographs. The 2D FFT provides an effective way to analyze the entire images and gives therefore, more representative values for LIPSS periods than singular values deduced from the SEM images.

III. RESULTS AND DISCUSSION

A. Frequency and orientation of the periodic structures

Figure 2 shows the typical results from this experimental set-up. These patterns are characterized by the period (Λ) and the orientation with respect to the incident beam polarization. Perpendicular LSFL, perpendicular HSFL and parallel HSFL are found for the range of laser fluences and scan speeds tested.

At 29 mJ·cm^{-2} (Figures 2(a)–2(d)), a scan speed of 0.1 mm·s^{-1} was required to start surface texturing (Figure 2(a)) with no evidence of material removal. A set of shallow grooves were formed parallel to the incident laser beam polarization, whose period increases as the scan speed decreases or the number of pulses applied increases (Figure 2(a) $\Lambda = 51$ nm and Figure 2(b) $\Lambda = 129$ nm). Furthermore, subwavelength apertures perpendicular to the beam polarization were printed with a period around 425 nm. By applying 1899 pulses (0.06 mm·s^{-1}), contact profilometry shows that these generated structures remain below the original surface level (crater depth of around 30 nm), evidencing a certain material ablation. This implies that the process has been performed slightly above the ablation threshold for the number of pulses applied.[19,20] By increasing the number of pulses up to 3796 pulses (scan speed of 0.03 mm·s^{-1}), deeper craters and deeper ripples appeared with periods between 275 to 315 nm and orientation perpendicular to the beam polarization, showed by the white arrows in the micrographs.

At a higher laser fluence, 53 mJ·cm^{-2} (Figures 2(e)–2(h)), much lower number of pulses (85 pulses) was needed to start surface corrugation and material ablation (crater depth of around 80 nm) (Figure 2(e)). While the lower energy density produces parallel ripples and subwavelength apertures at the first steps of surface modification, higher values of the irradiation fluences provide shallow perpendicular ripples with periods between 500–715 nm. By reducing the scan speed down to 0.1 mm s^{-1}, the depth of the perpendicular ripples increases (Figure 2(h)), and the period of the LIPSS decreased to 300 nm. So, at this high fluence regime, the transition from LSFL to HSFL perpendicular to the laser polarization was clearly observed.

The periods of the perpendicular LSFL and HSFL, calculated from 2D-FFT analysis, are summarized in Figure 3. Note that two different kinds of periodic gratings perpendicular to the laser beam polarization have been detected in the Nb samples. One corresponds to periods between 400 and 715 nm, assigned as LSFL or near subwavelength ripples, where the ratio of Λ to the laser wavelength (λ) in normal incidence takes values between 0.4 and 1.0. On the other hand, periodic structures with periods around 300 nm, namely HSFL or deep subwavelength ripples, appear with Λ/λ ratios lower than 0.4.

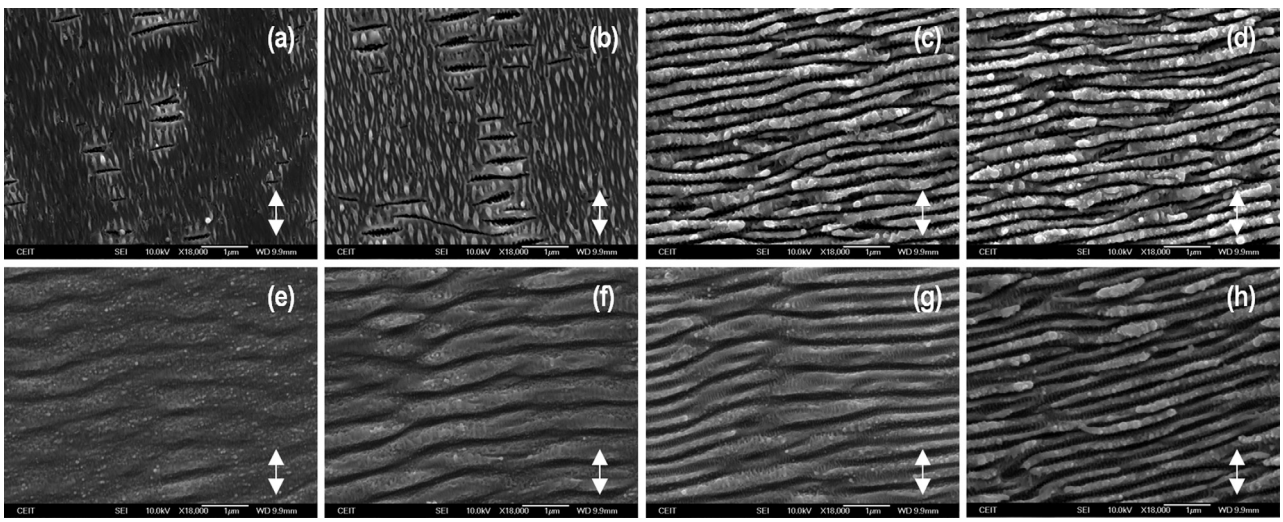

FIG. 2. FESEM images of the Nb surface after laser irradiation at fluences of 29 mJ·cm^{-2} from (a) to (d) and 53 mJ·cm^{-2} from (e) to (h). The number of pulses applied are (a) 1139, (b) 1898, (c) 3796, (d) 5694 pulses, (e) 85, (f) 142, (g) 284, and (h) 851 pulses. The arrow shows the polarization of the incident laser beam.

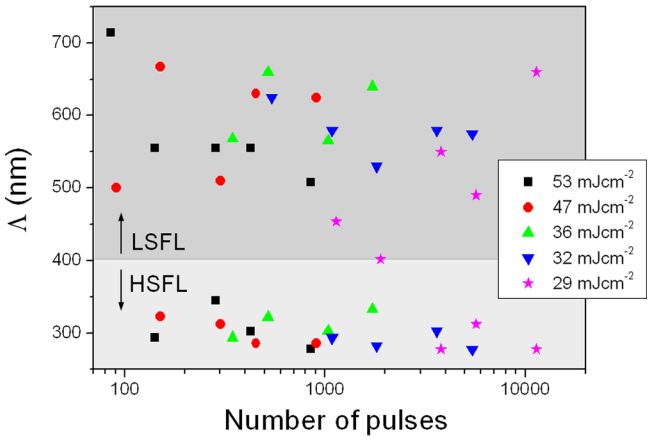

Fluence (mJcm^{-2})	Average number High Frequency Periods (nm)	Average number Low Frequency Periods (nm)
53	577±79	305±29
47	586±76	302±19
36	608±49	313±18
32	578±34	289±11
29	511±99	289±20

FIG. 3. Periods of the perpendicular LIPSS as a function of the number of pulses applied for each energy density tested and table summarizing the average number of high and low frequency periodicities measured for the different fluences.

Additionally, a LIPSS analysis was also carried out in the central and peripheral areas of the laser fingerprint. Both locations show the effects of irradiating at different energy density due to the Gaussian beam profile of the incident fs-laser, and different number of pulses since the circular laser spot overlapping.

Figure 4 presents the FESEM images of the Nb sample irradiated at 32 mJ·cm^{-2} with 1087 pulses (Figure 4(a)) and with 3623 pulses (Figure 4(b)). Applying 1087 pulses, the peripheral area shows HSFL parallel to the polarization with periods around 145 nm (Figure 4(a)), and the parallel ripples in the central area reduces their period down to 65 nm. An increase of the number of pulses applied (up to 3623 pulses), generates a transformation of the parallel HSFL in the peripheral area into nanodrops with round shape. Moreover, the ripples at the edge of the perpendicular ripples almost disappear to lead a nanobubble shape (Figure 4(b)). This tendency was observed at the whole range of laser fluence tested. Hence, the intensity and number of pulses threshold for the short parallel LIPSS is lower than that of the perpendicular LIPSS, since the former are generated even at the peripheral areas of the microstripes.

B. Transition from LSFL to HSFL perpendicular to the beam polarization

Since in some operation conditions both types of LSFL and HSFL perpendicular periodic structures appear simultaneously (Figure 3), a further analysis of the proportion of perpendicular ripples with low and high spatial frequency periods (near and deep subwavelength ripples) is carried out. In order to do this, the ratio of the peak areas of the corresponding periods on the 2D-FFT signals profiles were calculated and analyzed. Figure 5 depicts the peaks corresponding to the HSFL and LSFL periods (light and dark gray rectangles, respectively) on the Fourier Transform profile of the FESEM images corresponding to the Figures 2(f)–2(h). It is shown that, as the number of pulses applied increases, the ratio between LSFL and HSFL decreases. Therefore, the decrease of the feedrate results in a predominance of HSFL structures.

The I_{LSFL}/I_{HSFL} ratio was calculated for each irradiation condition, and the results are plotted in Figure 6 as a function of the number of pulses and allowed the definition of three different regimes:

1. For $I_{LSFL}/I_{HSFL} \geq 2$, surface gratings with a period around 600 nm is more frequent.
2. For $I_{LSFL}/I_{HSFL} \leq 0.5$, patterns with a more frequent 300 nm period appear.
3. For $0.5 < I_{LSFL}/I_{HSFL} < 2$, coexistence of both types of laser-induced ripples occurs.

It is clearly observed that the first regime, where the textured surface shows mainly a periodicity of 600 nm (see

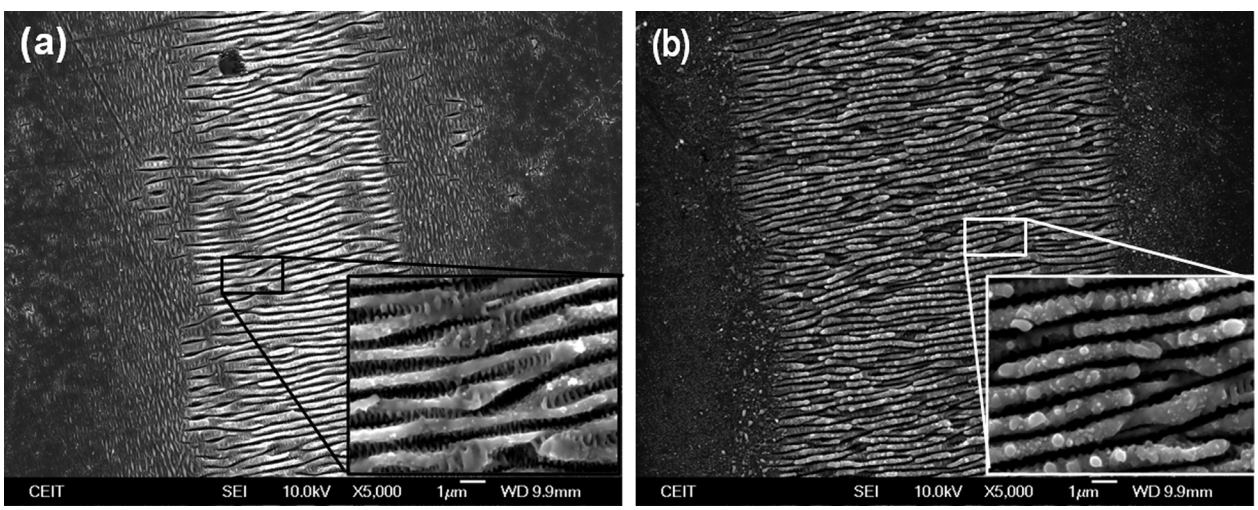

FIG. 4. FESEM micrographs of Niobium samples irradiated at (a) 32 mJ·cm^{-2} and 0.1 mm·s^{-1} (1087 pulses) and (b) 32 mJ·cm^{-2} and 0.03 mm·s^{-1} (3623 pulses). The insets show images at 18000× magnification of the central area.

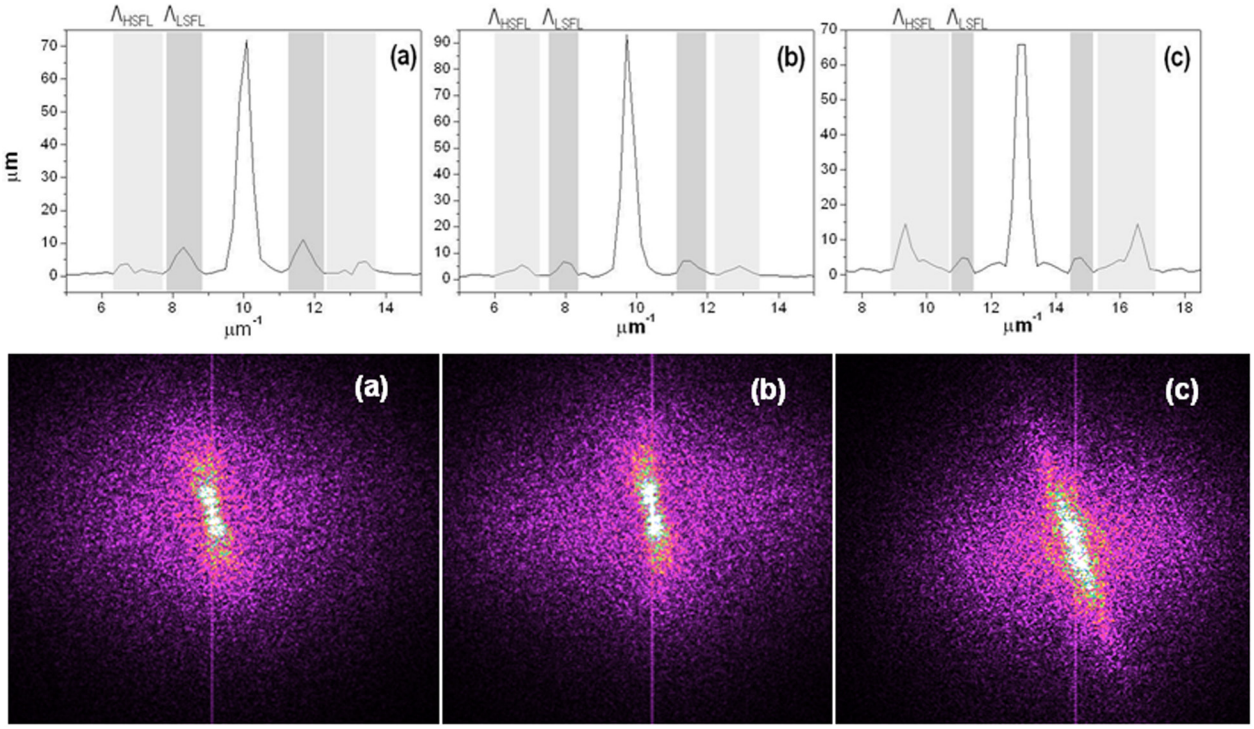

FIG. 5. 2D-FFT scattering graphs and their profiles obtained from the detailed images collected on Figures 2(f)–2(h). The light and dark gray rectangles delimit the peaks corresponding to the HSFL and LSFL periods, respectively. The irradiation fluence was 53 mJ·cm^{-2}, and the number of pulses was (a) 142, (b) 284, and (c) 851.

Figures 2(e) and 2(f)), corresponds to the samples processed at 53 mJ·cm^{-2} and 85 or 142 pulses (1.0 and 0.6 mm·s^{-1}). As the number of pulses is increased the generation of HSFL (300 nm) is enhanced up to 851 pulses (0.1 mm·s^{-1}), where the 300 nm period is more frequent. A similar behaviour was observed at lower energy densities (47 and 36 mJ·cm^{-2}); the transition from LSFL to HSFL takes place as the scan speed decreases or the number of pulses applied increases. Therefore, the number of pulses (and not the fluence) is the key parameter to control the period of the generated structures.

In summary, the average size of the perpendicular surface structures becomes smaller with an increasing number of laser pulses that leads to the formation of ripples with periods around 300 nm (HSFL) by the splitting of the main ridge of the low spatial frequency ripples. Moreover, in the ablation regime corresponding to high fluence, the transition between wavelength and subwavelength structures is observed by an intermediate step where the concurrence of both laser-induced ripples is observed.

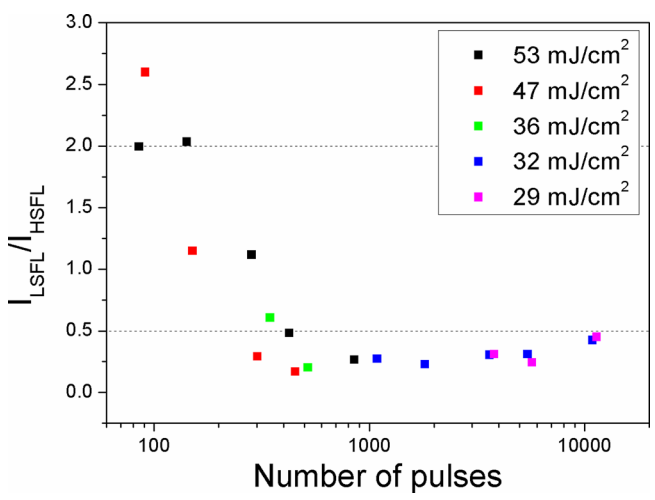

FIG. 6. Ratio of the peak areas of the laser-induced low and high spatial frequency LIPSS from the 2D-FFT as a function of the number of pulses.

So as to validate what was observed on the SEM images and to obtain the depth profile of the ripples, an intermediate structure formed by irradiating at 47 mJ·cm^{-2} and 0.3 mm·s^{-1} (302 pulses) presented in Figure 7(a) was further investigated by AFM. Figure 7(b) is an AFM 3D image of this intermediate structure where a combination of LSFL and HSFL is depicted. The AFM 3D cross section profile is presented in Figure 7(c). In this analysis, it is clearly visible that the main ridge of the LSFL ripple, located on the left, starts to split into two ridges. The splitting of the LSFL ridge provides a new ripple with a period around 300 nm (on the right side ripple).

The morphological evolution mechanism here presented is in agreement with the results reported in the literature.[3–5] By numerical simulations, Yao and Zhang establish that the interaction of the incident light with the metal surface will be modified after the formation of LSFL, leading to the redistribution of the electric field intensity on the metal surface. For shallow LSFL, the incident light will be localized in the valleys of the ripples resulting in a deepening and an elongation of the periodic pattern. This evolution can be observed in Figures 1(e)–1(g). When the depth of the grooves exceeds a certain value (around 150 nm in Figure 7(c)), the distribution of the electric field will be greatly changed, so the maxima of the electric field intensity will be

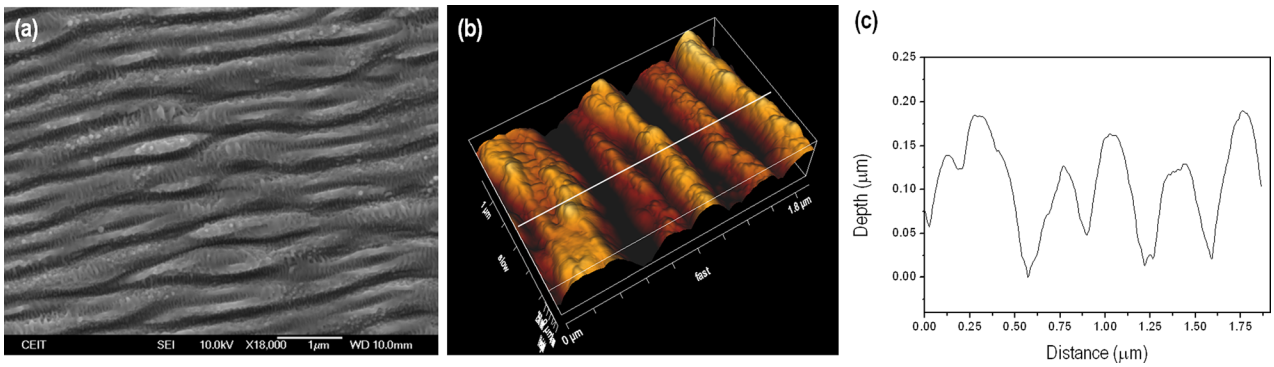

FIG. 7. AFM analysis of Niobium surface after femtosecond laser irradiation at 47 $mJ \cdot cm^{-2}$ and 0.3 $mm \cdot s^{-1}$ (302 pulses). (a) FESEM micrograph; (b) higher magnification AFM 3D image of (a); and (c) cross section profile by the line showed on (b).

localized on the top of the ripples, i.e., protuberance situated at both sides of the valleys. This feature will induce the split of the long periodic ripples and the generation of short periodic ripples.[3,5]

C. Physical models for the generation of periodic structures

In order to analyse the physical mechanism behind Nb surface structuring, we compare our experimental results with different models discussed in literature.

The classical theory or efficacy factor theory[21] considers the interference between the incident laser and the scattered light as the possible explanation of the periodic grating generation. By this theory, supposing a constant refractive index, the interspacing d of these periodic ripples is classically given by

$$d = \lambda/(1 \pm \sin\theta), \tag{1}$$

where λ and θ are the laser wavelength and the laser beam incidence angle measured from the surface normal, respectively. This is clearly observed for picosecond and nanosecond laser irradiation. Nevertheless, the LSFL periods obtained in the whole range tested by the femtosecond laser are shorter than the laser wavelength ($<0.9\lambda$). As expected, our experimental result does not follow this conventional prediction.

In order to explain the period reduction, several works[6–8] suggest the efficacy factor theory along a transient change of the refractive index (n). Skolski *et al.*[8] explain in alloyed steel the formation of parallel HSFL with periods between $\lambda/4$–$\lambda/8$ and the appearance of perpendicular LSFL with periods somewhat smaller than the incident laser wavelength. These results are in agreement with what observed in our samples. We observed the generation of parallel ripples with periodicity around 100 nm, which increases by the rise of the number of laser pulses applied, and also the formation of the perpendicular ripples with periods around 600 nm.

Currently, another explanation, which try to understand the "non classical" characteristics of the periodic gratings on metal surfaces obtained by multipulse femtosecond lasers irradiation, considers that the ripples result from the Surface Plasmons (SP)-laser interference and the subsequent grating-assisted SP-laser coupling.[9–13] The excitation of the plasmonic wave by incident laser wave should be fulfilled in our experiments, since the LIPSS reported correspond to a laser irradiation with a number of pulses equal or higher to 85. Therefore, the first several pulses could start texturing the Nb surface and then, subsequent pulses would cause the interference coupling with the surface plasmons.

According to this plasmonic model, for the normal incident laser, the plasmon wavelength at the metal/dielectric interface is given by[22]

$$\lambda_{SP} = \lambda \Re\left[\left(\frac{\varepsilon_d + \tilde{\varepsilon}_m}{\varepsilon_d \tilde{\varepsilon}_m}\right)^{1/2}\right], \tag{2}$$

where $\varepsilon_d = 1$ (complex dielectric constant of the dielectric), $\varepsilon_m = (n + i\kappa)^2$ is the complex dielectric constant of the metal, n is the real part of the refractive index of the metal, κ is the coefficient of extinction or imaginary part of the refractive index, and λ is the wavelength of the incident laser.

Considering the Niobium refractive index and extinction coefficient at 800 nm, $n = 2.15$, and $\kappa = 3.37$, respectively (measured by Weaver *et al.* in a mechanically and chemically polished Nb sample[23]), the value of the plasmon wavelength obtained ($\lambda_p = 769$ nm) is higher in comparison with most of the periods obtained in our irradiation experiments. However, the value of the refractive index was obtained from a smooth surface of single Nb crystals at room temperature, and, therefore, these values could not be suitable when the metals are heated by high intensity femtosecond laser pulses, and the Nb is already covered by nano and microstructures or an oxide compound. The roughness of the Nb surface increases the real part of the effective refractive index between the metal/air interface, and so the reduction of the ripple period will occur.[12] Besides, the interband transitions contribute to the absorption at frequencies well below 0.5 eV for the bcc transition metals,[24] so the combination of the Dudre model and the interband response must be taken into consideration to estimate the value of the dielectric constant ($\varepsilon_m = \varepsilon_D + \varepsilon_{IB}$). As it occurs with the Ni,[22] this interband contribution will slightly decrease the period compared to the one calculated from the dielectric constant, based upon only a Drude type absorption dependence.

However, among the perpendicular LIPSS obtained, we have not detected a period dependence with the laser fluence in the range tested (table on Figure 3). This insensitivity of

TABLE I. Range of number of pulses required to generate the LSFL and HSFL perpendicular and parallel to the beam polarization.

Fluence (mJ·cm^{-2})	LSFL ⊥	LSFL ⊥ + HSFL ⊥	HSFL ⊥	HSFL ∥
47–53	<145 pulses	145 < pulses < 300	300 < pulses < 855	…
36	< 200 pulses	200 < pulses < 500	>500 pulses	…
32	…	…	>1000 pulses	<550 pulses
29	…	…	>3790 pulses	<1900 pulses

the laser energy density on the period for both LSFL and HSFL differs from previous works based on the coupling of the SP and the laser light, where the interspaces become shorter near the ablation threshold as the laser energy fluence decreases.[14,25]

IV. CONCLUSIONS

In this work, it is reported for the first time the texturing of the Nb surface with LIPSS by femtosecond laser multi-pulse ablation in a range of laser fluences slightly above the ablation thresholds.

Attending the discussion involving the formation mechanism of LIPSS, two different stages can be observed on the corrugation of our metal surface: First, the generation of the perpendicular LSFL ($\Lambda_{LSFL_\perp} \approx 600$ nm) and the parallel HSFL ($\Lambda_{HSFL//} \approx 100$ nm), and second, the development of perpendicular HSFL which period is half of Λ_{LSFL} ($\Lambda_{HSFL_\perp} \approx 300$ nm). The morphological evolution mechanism that generates the HSFL due to the splitting in two of the LSFL is explained by the redistribution of the electric field intensity on the metal surface.

This method of micro/nanostructuring allows controlling the grating period by the number of laser shots applied (fixing the sample scan speed). Table I summarizes the ranges of number of pulses applied in order to obtain the LSFL and HSFL perpendicular to the beam polarization, the coexistence between both perpendicular structures and the parallel HSFL.

From our understanding, considering the insensitivity of the periods obtained with the laser fluence range tested and the impossibility of explanation of parallel HSFL by the plasmonic model, the most likely interpretation seems to be the efficacy factor theory along a transient change of the refractive index. However, more theoretical and experimental work would be required in order to establish an accurate physical model on the Nb surface texturing.

[1]L. Li, M. Hong, M. Schmidt, M. Zhong, A. Malshe, B. Huis in'tVeld, and V. Kovalenko, CIRP Ann. - Manuf. Technol. **60**, 735–755 (2011).
[2]A. Borowiec and H. K. Haugen, Appl. Phys. Lett. **82**, 4462–4464 (2003).
[3]J.-W. Yao, C.-Y. Zhang, H.-Y. Liu, Q.-F. Dai, L.-J. Wu, S. Lan, A. V. Gopal, V. A. Trofimov, and T. M. Lysak, Opt. Express **20**(2), 905 (2012).
[4]S. Hou, Y. Huo, P. Xiong, Y. Zhang, S. Zhang, T. Jia, Z. Sun, J. Qiu, and Z. Xu, J. Phys. D: Appl. Phys. **44**, 505401 (2011).
[5]W. Zhang, G. Cheng, Q. Fenga, L. Cao, F. Wang, and R. Hui, Appl. Surf. Sci. **257**, 4321–4324 (2011).
[6]Q. Wu, Y. Ma, R. Fang, Y. Liao, and Q. Yu, Appl. Phys. Lett. **82**, 1703 (2003).
[7]T. Q. Jia, Phys. Rev. B **72**, 125429 (2005).
[8]J. Z. P. Skolski, G. R. B. E. Römer, A. J. Huis in't Veld, V. S. Mitko, J. V. Obona, V. Ocelik, and J. T. M. De Hosson, in *LPM2010–the 11th International Symposium on Laser Precision Microfabrication*, 2010.
[9]Y. Vorobyev and C. Guo, J. Appl. Phys. **104**, 063523 (2008).
[10]J. Wang and C. Guo, J. Appl. Phys. **100**, 023511 (2006).
[11]S. Bashir, M. S. Rafique, and W. Husinsky, Nucl. Instrum. Methods Phys. Res. B **275**, 1–6 (2012).
[12]Y. Vorobyev, V. S. Makin, and C. Guo, J. Appl. Phys. **101**, 034903 (2007).
[13]G. Miyaji and K. Miyazaki, Opt. Express **16**(20), 16265–16271 (2008).
[14]M. Okamuro, M. Hashida, Y. Miyasaka, Y. Ikuta, S. Tokita, and S. Sakabe, Phys. Rev. B **82**, 165417 (2010).
[15]M. B. Nejad, Md. A. Mohamed, A. A. Elmustafa, P. Adderley, J. Clark, S. Covert, J. Hansknecht, C. Hernandez-Garcia, M. Poelker, R. Mammei, K. Surles-Law, and P. Williams, Phys. Rev. Spec. Top.–Accel. Beams **15**, 083502 (2012).
[16]S. Helali, A. Abdelghani, I. Hafaiedh, C. Martelet, M. I. Prodromidis, T. Albanis, and N. Jaffrezic-Renault, "Functionalization of niobium electrodes for the construction of impedimetric biosensors," Mater. Sci. Eng. C **28**, 826–830 (2008).
[17]M. Niinomi, M. Nakai, and J. Hieda, Acta Biomater. **8**, 3888–3903 (2012).
[18]R. Godley, D. Starosvetsky, and I. Gotman, J. Mater. Sci.: Mater. Med. **15**, 1073–1077 (2004).
[19]G. D. Tsibidis, M. Barberoglou, P. A. Loukakos, E. Stratakis, and C. Fotakis, Phys. Rev. B **86**, 115316 (2012).
[20]C. A. Zuhlke, T. P. Anderson, and D. R. Alexander, Opt. Express **21**, 8460–8473 (2013).
[21]J. E. Sipe, J. F. Young, J. S. Preston, and H. M. Van DrieL, Phys. Rev. B **27**(2), 1141–1154 (1983).
[22]F. Garrelie, J. P. Colombier, F. Pigeon, S. Tonchev, N. Faure, M. Bounhalli, S. Reynaud, and O. Parriaux, Opt. Express **19**(10), 9035–9043 (2011).
[23]J. H. Weaver, D. W. Lynch, and C. G. Olson, Phys. Rev. B **7**, 4311–4318 (1973).
[24]P. Romaniello, "Time-dependent current-density-functional Theory for metals," Ph.D. thesis (University of Groningen, Nijenborgh, 2006).
[25]S. Sakabe, M. Hashida, S. Tokita, S. Namba, and K. Okamuro, Phys. Rev. B **79**, 033409 (2009).